An Anisotropic Polarizable Water Model: Incorporation of All-Atom Polarizabilities into Molecular Mechanics Force Fields

Dan N. Bernardo, Yanbo Ding, Karsten Krogh-Jespersen, and Ronald M. Levy*

Department of Chemistry, Rutgers, The State University of New Jersey, New Brunswick, New Jersey 08903

Received: November 18, 1993; In Final Form: February 8, 1994®

An anisotropic polarizable water model has been constructed using atomic polarizabilities of oxygen and hydrogen and the SPC molecular mechanics force field. The presence of polarizable interaction sites on all atoms allows treatment of dipole–dipole interactions between bonded atoms and simplifies the incorporation of polarization treatments into existing molecular mechanics force fields. The resulting many-body potential yields the correct dipole moments for the water monomer and dimer as well as molecules in the bulk. Furthermore, the model predicts structures, energies, and dynamical behavior for bulk water which are in good agreement with experimental findings.

I. Introduction

Several potential energy functions for water are currently used in computer simulations of pure water and water–solute systems. Most simulations use potentials that are pairwise additive.[1] Calculations with many-body potentials[2-16] are not common partly due to the substantial increase in computational requirements demanded by such potentials. These potentials often express the many-body component of the potential energy function in terms of atomic and molecular polarizabilities. The development of such functions and their use in simulations requires development of new molecular mechanics force fields[2-6] or reparametrization of terms in the existing force fields.[7,8] Other approaches to polarization use either additional variable point charges[9-12] or multipole expansions of the electrostatic interaction.[13,14] Additional many-body potentials will undoubtedly be devised as ever increasing computational capabilities[17-19] encourage their use.

There is a need for an all-atom, many-body potential energy function which combines polarization effects within a framework compatible with existing molecular mechanics force fields. First, many-body polarization effects are presumed to be important for describing the energetics of interfacial phenomena,[20,21] some types of ionic[2,22-26] and hydrophobic solvation,[27-31] and cluster chemistry[32-35] to name a few applications, although it is not yet well established for which systems polarization must be included explicitly.[29,30] Second, by retaining other (nonelectrostatic) components of standard molecular force fields in the polarizable potential, it may be possible to build upon the large effort that has gone into the construction of existing molecular mechanics potential functions. With the polarizable potential it becomes possible to examine the many-body nature of the electrostatic interactions. Preservation of the nonelectrostatic pairwise terms simplifies the analysis involved when comparing predictions obtained with the polarizable potential to those calculated using pairwise potentials.

The development and evaluation of a many-body potential along the lines described above is the main objective of this study. A polarizable potential must be able to predict polarizabilities for any given configuration of atoms in a condensed-phase molecular system. We also require that, for small molecules, the gas-phase molecular polarizability be reproduced by our polarizable model. Methods for calculating molecular polarizabilities have been published;[36-38] in this paper we shall discuss the incorporation of such a method into the existing framework of molecular mechanics force fields. We shall also examine some computational issues associated with the use of the resulting potential, since it is well known that the evaluation of many-body functions is computationally demanding.

II. Theory

In this section we outline the procedure for calculating molecular polarizabilities and the many-body polarization energy. We also discuss the modifications needed in order to incorporate the polarization terms into the widely used SPC model[39] for water. For the resulting hybrid force field, the total potential energy of the system can be written as

$$U_{tot} = U_{pair} + U_{pol} \tag{1}$$

The pairwise term, with the exception of the values for the partial atomic charges, arises solely from the SPC model and uses the following function to describe the Lennard-Jones and Coulomb interactions between water molecules:

$$U_{pair} = \sum_{i,j} 4\epsilon_{ij}\left[\left(\frac{\sigma_{ij}}{r_{ij}}\right)^{12} - \left(\frac{\sigma_{ij}}{r_{ij}}\right)^{6}\right] + \frac{q_i q_j}{r_{ij}} \tag{2}$$

Here, r_{ij} is the distance between atoms i and j, q_i and q_j are partial atomic charges, and ϵ_{ij} and σ_{ij} are constants.[39] Note that no bond length or angle energy terms are included in the potential since each water molecule is assigned a fixed O–H bond length of 1.0 Å and a fixed H–O–H bond angle of 109.5°. In order to reproduce the gas-phase dipole moment[40] of 1.855 D, the charges on the oxygen and hydrogen atoms are chosen[8] as $q_O = -0.6690$ and $q_H = 0.3345$.

The polarization energy U_{pol} is obtained by[41,42]

$$U_{pol} = {}^1/_2 \sum_i \mu_i E_i^0 \tag{3}$$

Given the electrostatic field due to the permanent charges E_i^0, the induced dipole moments μ_i can be obtained by any of several procedures developed to predict molecular polarizabilities.[38] These procedures are based on the atom–dipole interaction model,[43] and require atomic coordinates and atomic polarizabilities as input. The values of the latter are chosen to minimize the differences between the calculated and experimental molecular polarizabilities for a number of test molecules. Most of the methods assign different values of the atomic polarizability to atoms that have different molecular environments.[38] These methods are good at describing the polarizability of a single, isolated molecule with a well-defined structure. However, it is not clear how well they would describe polarizabilities in the

® Abstract published in *Advance ACS Abstracts,* March 15, 1994.

0022-3654/94/2098-4180$04.50/0

condensed phase where interatomic distances are continuously variable and where distances between highly polar and/or ionic groups are on the order of bonding distances. For example, the procedure described by Applequist and co-workers[37] assigns a specific value to the atomic polarizability of a carbonyl oxygen. This value does not change even if a hydrogen atom on a neighboring molecule approaches the oxygen, and at sufficiently small interatomic distances the induced dipoles on the two atoms will approach unreasonably large values. Situations such as these can be avoid by damping the atomic polarizabilities for atoms that are close to each other. The damping can be thought of as a decrease in the atomic polarizabilities at short distances due to the overlap of electronic charge distributions.

Such a damping procedure is used in a method proposed by Thole[36] for calculating molecular polarizabilities from atomic constituents. This method uses values for atomic polarizabilities which are close to the *ab initio* and/or experimental values.[44] Furthermore, only one value of the atomic polarizability for a given element is used regardless of its chemical environment. While the valence state of the atom certainly affects the polarizability, the differences in polarizability arise from the local bonding geometry as it affects the damping. This transferability of atomic polarizabilities makes the Thole approach attractive since, in keeping with the philosophy behind molecular mechanics force fields, it can be applied to a wide variety of molecules.

We now briefly review the procedure for calculating the induced dipole moments and forces on the atoms. If the polarizability tensor of atom i is α_i, then the induced dipole moment μ_i is given by

$$\mu_i = \alpha_i(\mathbf{E}_i^0 - \sum_{j \neq i} \mathbf{T}_{ij}\mu_j) \tag{4}$$

The dipole field tensor $\mathbf{T}_{ij}$ is calculated as follows. It is first necessary to introduce a damping function which acts only at short distances where the electronic distributions are poorly approximated by point charges. To do this, Thole first assumes that an atom of unit polarizability has a conical electronic charge density with a radius of 1.662 Å. A scaling distance is defined as

$$s_{ij} = 1.662(\alpha_i\alpha_j)^{1/6} \tag{5}$$

and the distance between two atoms is then scaled as

$$v_{ij} = \begin{cases} r_{ij}/s_{ij} & \text{if } r_{ij} < s_{ij} \\ 1 & \text{otherwise} \end{cases}$$

The problem with the above equation is that $\partial v_{ij}/\partial r_{ij}$ is discontinuous at $r_{ij} = s_{ij}$, which causes problems when forces due to polarization are evaluated. This discontinuity can be removed by replacing v_{ij} with a new scaling function

$$w_{ij} = \begin{cases} \dfrac{r_{ij}}{s_{ij}} + \dfrac{1}{m}\left[1 - \left(\dfrac{r_{ij}}{s_{ij}}\right)^m\right] & \text{if } r_{ij} < s_{ij} \\ 1 & \text{otherwise} \end{cases} \tag{6}$$

where m is a constant. The value of m is dictated by the condition that the difference between w_{ij} and v_{ij} be sufficiently small for all physically reasonable values of r_{ij}. For this purpose we require that $(w_{ij} - v_{ij})/v_{ij} \leq 5\%$ for $0.5 < r_{ij}/s_{ij} < 1.0$, which we found empirically leads to[45] $m \geq 32$. The additional computational time required to evaluate large exponents in eq 6 is insignificant when compared to other computations during the simulations, and we have consequently set $m = 32$.

After the scaled distance is obtained using eq 6, the dipole field tensor can be evaluated via[36]

$$\mathbf{T}_{ij} = \frac{4w_{ij}^3 - 3w_{ij}^4}{r_{ij}^3}\mathbf{I} - \frac{3w_{ij}^4}{r_{ij}^5}\begin{bmatrix} x^2 & xy & xz \\ xy & y^2 & yz \\ xz & yz & z^2 \end{bmatrix} \tag{7}$$

where $\mathbf{I}$ is the identity matrix and x, y, and z are the Cartesion components of r_{ij}. The tensors for different pairs of atoms can then be substituted into eq 4 which, after rearranging, can be written in matrix form as

$$\begin{bmatrix} \alpha_1^{-1} & \mathbf{T}_{12} & \dots & \mathbf{T}_{1N} \\ \mathbf{T}_{21} & \alpha_2^{-1} & \dots & \mathbf{T}_{2N} \\ \vdots & \vdots & \ddots & \vdots \\ \mathbf{T}_{N1} & \mathbf{T}_{N2} & \dots & \alpha_{N-1} \end{bmatrix}\begin{bmatrix} \mu_1 \\ \mu_2 \\ \vdots \\ \mu_N \end{bmatrix} = \begin{bmatrix} \mathbf{E}_1^0 \\ \mathbf{E}_2^0 \\ \vdots \\ \mathbf{E}_N^0 \end{bmatrix} \tag{8}$$

or briefly

$$\mathbf{A}\mu = \mathbf{E}^0 \tag{9}$$

Once $\mathbf{A}$ is constructed, μ can be obtained by matrix inversion

$$\mu = \mathbf{A}^{-1}\mathbf{E}^0 \tag{10}$$

or by iterative solution of eq 4. Knowledge of μ then allows evaluation of U_{pol} as well as the forces on the atoms. The forces due to the dipole–monopole and dipole–dipole interactions are calculated using the expression[7,46]

$$\mathbf{F}_k = \sum_i \mu_i(\nabla_k \mathbf{E}_i^0) - {}^1/_2 \sum_i [\mu_i \sum_j (\nabla_k \mathbf{T}_{ij})\mu_j] \tag{11}$$

Preliminary simulations revealed that the induced dipoles become unrealistically large when two atoms are close to each other if the expression $E_i^0 = (1/4\pi\epsilon_0)\sum_j(q_j/r_{ij}^2)$ is used to calculate the field. This is due to the treatment of the atoms as point charges even at small r_{ij}. At these distances the electronic charge distributions are poorly represented by point charges, and some distance-dependent attenuation or shielding of the these charges is required. The need for such an attenuation has been recognized in several studies,[4,10,47] and in this paper it is done in conjunction with the damping of the dipole tensor at short distances (eq 6). Thole's suggestion[36] of $q'_j = (4v_{ij}^3 - 3v_{ij}^4)q_j$ does not sufficiently attenuate the field. Instead, the field is evaluated using

$$E_i^0 = \frac{1}{4\pi\epsilon_0}\sum_j \left\{1 - \exp\left[-\gamma\left(\frac{r_{ij}}{s_{ij}}\right)^n\right]\right\}\frac{q_j}{r_{ij}^2} \tag{12}$$

for all values of r_{ij}. The constants γ and n determine the extent of attenuation. The value of n is obtained as follows: Since the unattenuated field behaves as $1/r_{ij}^2$, Stillinger and David[4] determined that the attenuation function should behave as $r_{ij}^3 + O(r_{ij}^4)$. This would force E_i^0 to behave as r_{ij} at small distances, and the dipole moment induced at atom i by the field due to atom j would approach zero for small r_{ij}. Thus, the value $n = 3$ is used. The other attenuation parameter, γ, is then set to 0.85 in order to yield a reasonable value for the total potential energy of bulk water.

It must be noted that in evaluating eq 12 the contributions from 1–2 and 1–3 bonded interactions are not included. This restriction is made in an attempt to be consistent with existing molecular mechanics treatments of electrostatic interactions, which omit the Coulomb terms arising from these bonded interactions. In contrast, all dipole–dipole interactions, including the 1–2 and 1–3 components, are included in the evaluation of

TABLE 1: Parameters Used in the Polarizable Force Field[a]

atom	σ, Å	ϵ, kcal/mol	q^b	α, Å^3
O	3.166	0.1554	−0.6690	0.862
H	0.0	0.0	0.3345	0.514

[a] Note: Combining rules are $\sigma_{ij} = (\sigma_i + \sigma_j)/2$ and $\epsilon_{ij} = (\epsilon_i\epsilon_j)^{1/2}$. The distances for SPC water are r(OH) = 1.0 Å and r(HH) = 1.633 Å. [b] Electronic charge.

TABLE 2: Energy and Geometry of the Minimum-Energy Configuration of the Water Dimer

	polarizable model	SPC model	experiment[a]
U_{pot}, kcal/mol	−4.98	−6.60	−5.40 ± 0.70
R_{OO}, Å	2.80	2.74	2.98
θ_d, deg	53	52	51 ± 10
θ_a, deg	19	22	57 ± 10

[a] From refs 49 and 50.

eq 7. This is necessary since omission of the above components will lead to physically unrealistic predictions for the molecular polarizability.

Finally, it is interesting to note that the scaling functions used in T_{ij} and E_i^0 are important from both physical and computational points of view. They "smear out" the electronic charge at small interatomic distances and thus prevent the occurrence of abnormally large induced dipoles.

III. Results and Discussion

Molecular dynamics simulations of water were performed using the IMPACT program[48] and the SPC model geometry and Lennard-Jones parameters.[39] The atomic charges, atomic polarizabilities, and various other parameters used in the force field are summarized in Table 1. Most simulations were carried out on a system of 216 water molecules. The energetics and behavior of the induced dipoles were studied. In addition, radial distribution functions and other bulk properties of water were calculated. Comparisons of bulk properties with those of small water clusters were also carried out. The predictions of the polarizable model were also compared to those of the SPC model. The permanent dipole moment of the SPC model is 2.27 D. In contrast, the polarizable model gives the correct gas-phase dipole moment (solely due to the permanent charges) of 1.855 D. This dipole moment is due to the fixed charges assigned to the atomic centers; there is no induced dipole moment for the monomer since, in the framework of the model, electric fields due to 1–2 and 1–3 bonded interactions are not considered. Effects of polarization become apparent only in the water dimer and larger clusters.

A. Calculations for the Water Dimer and Trimer. The potential energy surface of the water dimer was investigated by varying the oxygen–oxygen distance R_{OO} and leaving all remaining geometrical variables unconstrained. The energy minimum of U_{tot} = −4.98 kcal/mol was found at R_{OO} = 2.80 Å. The polarization energy is −1.01 kcal/mol, which is 20% of the total potential energy. Comparisons of these values with those predicted by the SPC model and experimental data are made in Table 2. The minimum energy for the present model is comparable to the experimental value which is −5.40 kcal/mol. The SPC model, on the other hand, predicts a deeper minimum of −6.60 kcal/mol. This is due to the larger molecule dipole moment inherent to this model, which has been optimized to yield bulk properties. The intermolecular oxygen–oxygen distance in the water dimer for both SPC and the present model is smaller than the experimental value of 2.98 Å.

The minimum-energy configuration for the water dimer is shown in Figure 1 while various distances and angles are summarized in Table 2. Note that θ_a, the angle between the O–O vector and the C_2 axis of the acceptor molecule, is too small in the geometries predicted by both models. This has been attributed[8] to the lack of directionality on the oxygen site of a three-center interaction model. Since the minimum-energy geometries from the simulations are different from the experimental geometries, one cannot compare the dipole moments at the minimum-energy geometry predicted by the two models to the experimental value. In order to make an approximate comparison, we have calculated $\mu_\parallel$ and $\mu_\perp$ (components of the dipole moment along and perpendicular to the oxygen–oxygen axis) for a dimer which possesses the experimental geometry; results are shown in Table 3. The SPC model, with its enhanced permanent dipole moment, overestimates $\mu_\parallel$ for the dimer. On the other hand, the agreement between the values predicted with the polarizable model and the experimental value is reasonable for both $\mu_\parallel$ and $\mu_\perp$ at this geometry.

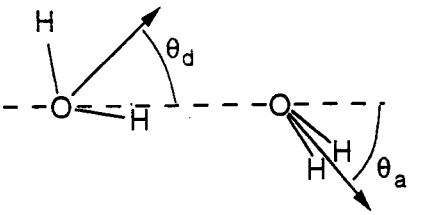

Figure 1. Minimum-energy configuration for the water dimer.

TABLE 3: Dipole Moments for the Experimental Minimum-Energy Configuration of the Water Dimer

	polarizable model	SPC model	experiment[a]
$\mu_\parallel$, D	2.64	3.67	2.6
$\mu_\perp$, D	0.19	0.19	0.4

[a] From ref 49.

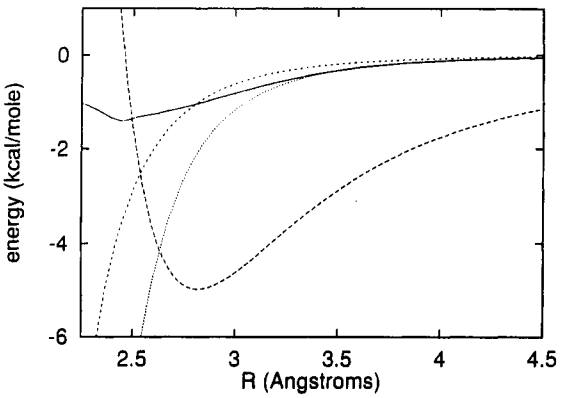

Figure 2. Minimum-energy surface of the water dimer as a function of the oxygen–oxygen distance. The long-dashed line denotes the total potential energy. The solid line represents the polarization energy U_{pol}. This quantity is obtained by attenuating E_i^0 and using Thole's procedure for calculating the induced dipoles. Failure to attenuate E_i^0 results in values of U_{pol} denoted by the dotted line. Use of Applequist's procedure for calculating the induced dipoles, combined with unattenuated values of E_i^0, yields U_{pol} as denoted by the short-dashed line.

The contribution of the polarization component to the energy surface of the dimer is shown in Figure 2. The polarization energy becomes more important with decreasing intermolecular distance. At short distances, however, the polarization energy is reduced as a result of the attenuation of E_i^0 (see eq 12). Failure to perform this attenuation leads to unreasonably large values of U_{pol} at oxygen–oxygen distances below 2.8 Å. This is observed in spite of the fact that another form of distance scaling (eq 6) is already done in the Thole procedure for calculating polarizabilities. Use of Applequist's method[37] in lieu of the Thole procedure results in the same qualitative behavior of U_{pol}. This behavior is not the artifact of a particular algorithm used to calculate polarizabilities; it is instead caused by unusually large values of E_i^0 at small interatomic distances. This situation is avoided by attenuating E_i^0 when the distances between polarizable interaction sites become small.

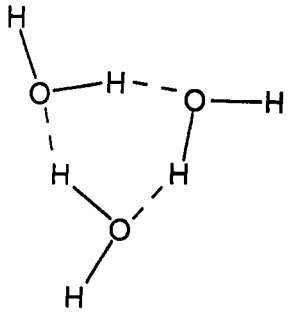

Figure 3. Minimum-energy configuration for the water trimer.

TABLE 4: Structural Parameters for the Water Trimer

	polarizable model	SPC model	experiment[a]
R_{OO}, Å	2.74	2.75	2.94, 2.97, 2.97
δ(O–H···O), deg[b]	166	166	150, 152, 153

[a] From ref 51. [b] Hydrogen bond angles, with $\delta = 180°$ corresponding to a linear hydrogen bond.

The presence of polarizable interaction sites means that the current model can offer new insights into the effects of polarizability as well as the differences between induced and permanent dipoles. For example, the simulations predict that the induced and permanent dipoles for a dimer complex in the minimum-energy configuration will both be pointing along the oxygen–oxygen axis. The same alignment (i.e., nearly parallel) is observed for the induced and permanent dipoles on the acceptor molecule. On the other hand, the induced dipole on the donor molecule makes an angle of 60° with its permanent dipole. This is easily explained by examining the geometry as shown in Figure 1. The permanent dipole of the donor molecule is oriented along the H–O–H angle bisector. The induced dipole is mainly due to polarization of the hydrogen atom which participates in the hydrogen bond. The electrostatic field at this atom causes the induced dipole to be oriented along the hydrogen bond, which makes an angle of about 60° with the permanent dipole.

It was previously noted that although the polarizable model predicts the correct dipole moments for a dimer in the experimental configuration, it does not give the correct acceptor angle θ_a. This calls into question its ability to predict the structure of small water clusters. To test this, we have calculated the minimum-energy configuration for the water trimer as predicted by the polarizable model. The experimental optimal structure of the trimer[51] is cyclic with nearly linear hydrogen bonds as shown in Figure 3. Simulations using the polarizable model and the SPC model predict the same structure and similar structural parameters as summarized in Table 4. Both sets of simulations and the experiment show that all three hydrogen atoms which participate in hydrogen bonding are in the plane formed by the three oxygen atoms. In summary, the polarizable model predicts a reasonable structure for the trimer, and in the following section it is shown that the model predicts the correct structure in the bulk as well.

B. Simulations of Bulk Water. Simulations were performed on a box of 216 water molecules with a density of 1 g/cm^3. Periodic boundary conditions were enforced. A spherical molecular cutoff of 8.5 Å was used in evaluating the pair potential functions. No cutoff was used in calculating the induced dipole moments, although use of a cutoff will be discussed later in this section. The induced dipole moments were obtained via inversion of the dipole tensor matrix A at every time step, which was set to 2.0 fs. The temperature was maintained at 298 K by applying a velocity rescaling approach proposed by Berendsen and co-workers[52] with a relaxation time of 10 fs. The system was equilibrated for 1 ps (large variations in the potential energy were no longer observed after the first 0.5 ps), after which we sampled the system for 10 ps. Simulations were run on a Thinking Machines Corp. CM-5 computer with 256 nodes; performance issues are discussed in a later section.

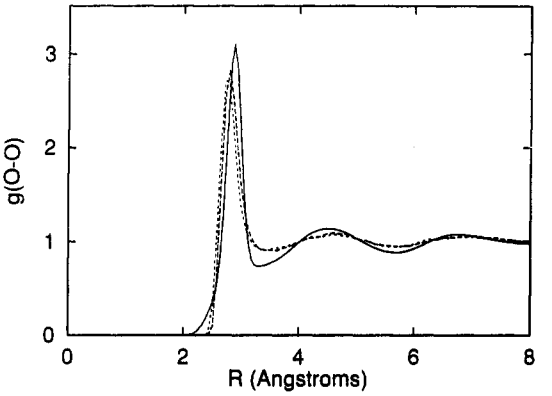

Figure 4. Oxygen–oxygen radial distribution functions. The dotted line is g_{OO} as predicted by the polarizable model; the dashed line is the result using the SPC model. The solid line denotes the experimental result.

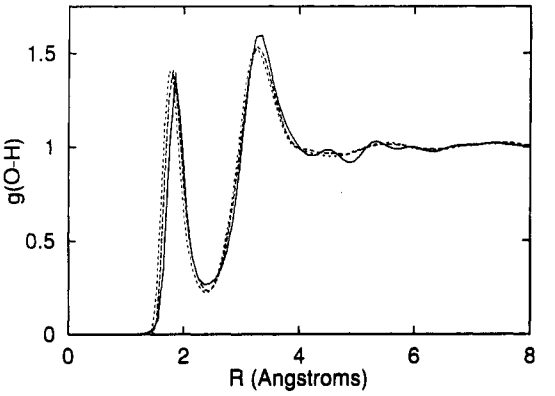

Figure 5. Oxygen–hydrogen radial distribution functions. The dotted and dashed lines are from the polarizable model and the SPC model, respectively. The solid line denotes the experimental result.

1. Structure. The oxygen–oxygen radial distribution function (g_{OO}) from our simulations is shown in Figure 4. Also shown are the experimental distributions obtained by Sopher and Phillips[53] as well as those predicted by simulations using the SPC potential. There is good general agreement between theory and experiment as far as the positions of the first and second maxima are concerned, although the first peak in the polarizable model's distribution corresponds to an O–O distance that is 0.10 Å smaller than the experimental result. The height of the first peak is also lower for the simulations than it is for the experiment. While there are differences in the detailed structure of g_{OO}, the number of neighbors in the first coordination shell is similar for all three data sets. Integration of g_{OO} up to 3.3 Å yields 4.4 neighbors for the experimental data and 4.2 neighbors for both sets of simulation results.

The presence of hydrogen bonds is perhaps better seen in g_{OH}, the oxygen–hydrogen radial distribution function. The theoretical and experimental results for this function are shown in Figure 5. All three distributions have nearly identical peak heights and positions. Integration of the first peak (up to 2.4 Å) yields the number of hydrogen bonds per molecule, which turns out to be 3.9 for the SPC model and 3.8 for both the experimental results and our model. The good agreement between all three data sets is again apparent in the hydrogen–hydrogen radial distribution function, g_{HH}, which is shown in Figure 6.

The cosine distribution of the water–water hydrogen bond (O–H···O) angle is shown in Figure 7. Only hydrogen bonds with lengths less than 2.40 Å (corresponding to the first minimum in g_{OH}) were considered in constructing this distribution. Both the polarizable model and the SPC model predict that most of the hydrogen bond angles are close to 180°.

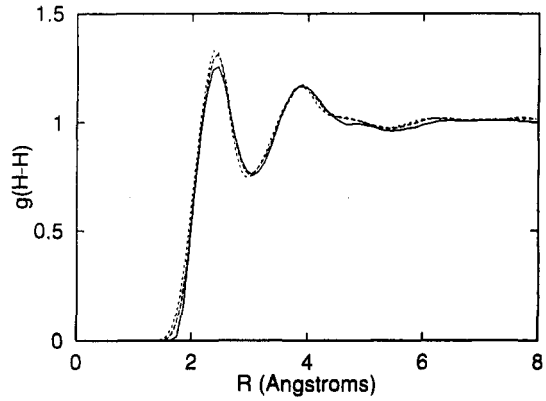

Figure 6. Hydrogen–hydrogen radial distribution functions. The dotted and dashed lines are from the polarizable model and the SPC model, respectively. The solid line denotes the experimental result.

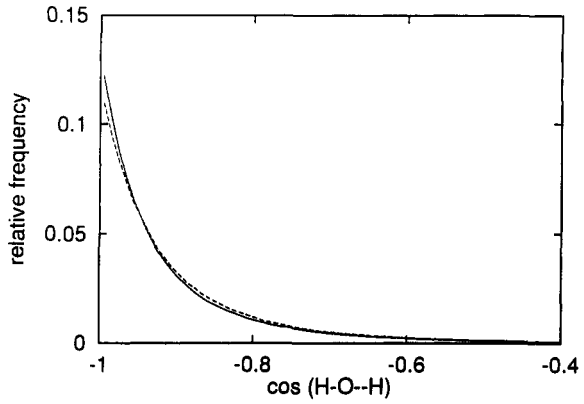

Figure 7. Cosine distributions of the water–water hydrogen bond (O–H···O) angle. The solid line denotes the distribution of the polarizable model, while the dashed line denotes that of the SPC model. These distributions represent configurations wherein a hydrogen atom forms a hydrogen bond with an oxygen atom on a neighboring molecule. Only hydrogen bonds with lengths less than 2.40 Å (corresponding to the first minimum in g_{OH}) are considered. Data for $\cos\theta > -0.4$ are not shown since there are very few configurations with these angles.

In summary, the structure of bulk water as predicted by the polarizable model is very similar to the structure determined by experiment and that predicted by the SPC model. The addition of the many-body polarization component to the potential energy function preserves the general tetrahedral structure of the liquid, including the number of first-shell neighbors and the number of hydrogen bonds. However, although the structures predicted by the polarizable model and by the SPC model are nearly identical, there are significant differences in the computed electrostatic properties.

Most potentials used in molecular mechanics simulations treat electrostatic interactions only by assigning permanent charges to various sites on a molecule. The resulting dipole moment is invariant to changes in the molecular environment, and any polarization of the molecule is assumed to be approximated in an "average" manner by the potential function. The SPC model is one such potential, and its atomic charges were chosen in order to reproduce the properties of bulk water. As a result, each molecule has a total dipole moment of 2.27 D regardless of the surrounding medium. In contrast, the total dipole moment of the polarizable model varies in response to the environment. The partial atomic charges on the atoms were chosen[8] to reproduce the experimental value of $\mu = 1.855$ D in the gas phase. When placed in the bulk the molecule becomes polarized, and the simulations predict an average induced dipole moment of 1.00 D contributing to the total dipole moment[54] of 2.81 ● 0.25 D. This is in the general range of dipole moments obtained in other molecular mechanics simulations,[3,10,13,39,55] which range from 2.27 to 2.9 D, and experimentally estimated dipole moments for ice,

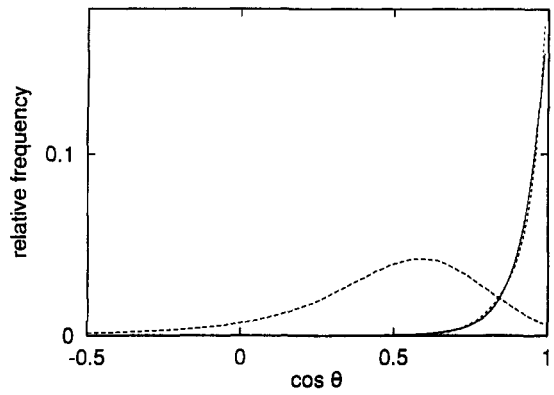

Figure 8. Cosine distributions of induced dipoles. Angles are evaluated with respect to the molecular C_2 axis. The dashed line represents the distribution of dipoles on the hydrogen atoms. This distribution has $\langle\cos\theta\rangle \approx 0.5$, which corresponds to an angle of 60°. The solid line represents the distribution of dipoles on the oxygen atoms, while the dotted line corresponds to the distribution of the induced dipole for the whole molecule. Data for $\cos\theta < -0.5$ are not shown since all distributions approach zero in this region.

TABLE 5: Dipole Moment Components of Water Molecules in the Bulk

component	value, D
induced dipole moment on O	0.65 ± 0.19
induced dipole moment on each H	0.31 ± 0.15
total induced dipole moment	1.00 ± 0.25
permanent dipole moment	1.85
total dipole moment	2.81 ± 0.25

values of which are usually[56–58] between 2.45 and 2.72 D but go as high as Onsager and Dupuis' esimate[59] of 3.61 D. The significant variation in our calculated dipole moment is not unexpected and is due to variations in the electrostatic fields experienced by the water molecules in solution. The sensitivity of the polarizable potential to changes in the electrostatic environment and the fact that it predicts enhanced dipole moments for water molecules in the bulk as well as the correct dipole moments for the water monomer and dimer suggests that the polarizable model will be useful in studies such as those of interfacial phenomena[20,21] and dielectric properties.[60,61]

Since each molecule has polarizable sites on all its atoms, the induce molecular dipole moment can be decomposed into its atomic components; each of these components is listed in Table 5. The induced dipole moments on the hydrogen atoms are considerable. This is a significant difference between our model and others which only treat the oxygen atom as the polarizable site. Furthermore, the induced dipoles on the atoms can point in different directions in response to differences in the local electrostatic fields. This is apparent in Figure 8, where the cosine distribution of the induced atomic dipoles with respect to the molecular C_2 axis is shown. The distribution for the induced dipoles on the hydrogen atoms is broad, with its maximum at a position corresponding to an angle of about 60°. This means that the induced dipoles on the hydrogen atoms are, on the average, usually oriented along the O–H bonds. On the other hand, the induced dipole on the oxygen atom is usually aligned with the molecular axis. Summation of the induced dipoles on the atoms yield the total induced molecular dipole. Although the induced dipoles on the hydrogen atoms are usually offset from the molecular axis by 60°, their off-axis components roughly cancel each other when the summation is performed and leads to an induced molecular dipole usually aligned with the molecular axis (coincident with the permanent dipole vector). Indeed, Figure 8 shows that there are very few instances where the angle between induced and permanent dipoles in the bulk is close to 60°.

The orientation of the induced molecular dipole moment μ_i with respect to the molecular geometry can be further examined

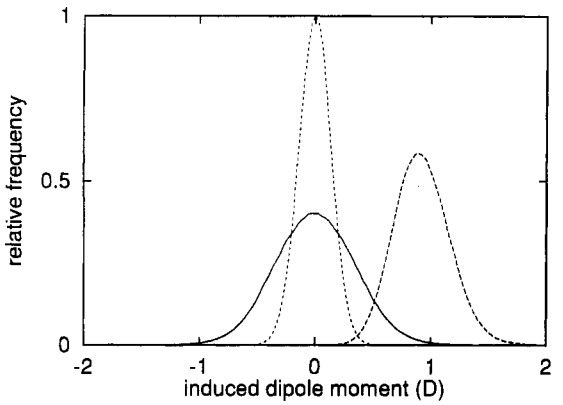

Figure 9. Projections of the induced molecular dipole moment onto the molecular coordinate axes. The dashed line is the projection onto the molecular C_2 axis. The dotted and solid lines represent the projections onto the H–H and out-of-plane axes, respectively.

if the dipole moment is projected onto a molecular coordinate system. A suitable coordinate system is defined by the molecular C_2 axis, an H–H axis, and an axis normal to the plane of the molecule. The projections of μ_i onto these axes are shown in Figure 9. The component of μ_i along the C_2 axis is by far the largest of the three. It is interesting to note that the component of μ_i which is normal to the plane of the molecule is more widely distributed than the component along the hydrogen–hydrogen axis. This anisotropy may be partly responsible for differences in the rotational motion about the three defined molecular axes, which will be examined later.

2. Energetics. The average total potential energy per water molecule in our simulations was found to be -9.58 ± 0.13 kcal/mol, which is close to the experimental value of -9.92 kcal/mol.[39] The average polarization energy is -3.74 ± 0.11 kcal/mol, which constitutes 39% of the total potential energy. This is considerably greater than the U_{pol}/U_{tot} ratio of 20% computed for the dimer. The increased role of polarization in the energetics of bulk water is one manifestation of the many-body interactions that are modeled with the potential. It must be noted that most of the polarization energy results from dipole–charge and dipole–dipole interactions at close range. The polarization energy scales as $1/r_{ij}^4$, whereas the longer-ranged Coulomb energy (the other major component of U_{tot}) varies with distance as $1/r_{ij}$.

The significant contribution of U_{pol} to U_{tot} is also observed in other many-body potentials whose treatments of electronic charge distributions and interactions are different from ours. The NEMO potential[3] uses charge distributions and polarizabilities based on the results of *ab initio* calculations and predicts $U_{pol}/U_{tot} = 44\%$. The polarizable electropole model,[13] on the other hand, uses no atomic charges. It represents the charge distribution by a multipole expansion using the experimentally obtained gas-phase dipole moments and molecular polarizability as well as quadrupole moments obtained from quantum mechanical calculations. For this model, $U_{pol}/U_{tot} \approx 31\%$. Note that the ratio of U_{pol} to U_{tot} is similar for all three potentials. For these many-body potentials, polarization effects make a significant contribution to the total energy for bulk water.

3. Dynamics. We have analyzed the transport properties of our all-atom polarizable model. The results of our simulations were used to obtain mean square displacements, which are related to the diffusion coefficient D via the Einstein relation

$$D = \frac{1}{6}\lim_{t\to\infty}\frac{d}{dt}\langle|R_i(t) - R_i(0)|^2\rangle \qquad (13)$$

Here, $R_i(t)$ is the position of the center of mass of molecule i at time t. The resulting diffusion coefficients for the polarizable model and the SPC model are shown in Table 6. The diffusion coefficient of SPC water (4.4 m^2/s) is too large, whereas that of the polarizable model (2.8 m^2/s) is much closer to the experimental value of 2.3 m^2/s. Apparently, the addition of induced dipoles slows the translational motion of a molecule[3] in the bulk and causes D for the polarizable model to approach the experimental value.

TABLE 6: Transport Properties of Water

	polarizable model	SPC	experiment
D, m^2/s	2.80 ± 0.10	4.4 ± 0.1	2.3[a]
correlation times,[b] ps			
$\tau_\mu^{(1)}$	4.74 ± 0.14	3.38 ± 0.22	3.8–5.0[c]
$\tau_{hh}^{(1)}$	3.65 ± 0.22	3.00 ± 0.27	
$\tau_{oopl}^{(1)}$	2.47 ± 0.14	2.17 ± 0.14	
$\tau_\mu^{(2)}$	2.15 ± 0.06	1.31 ± 0.04	
$\tau_{hh}^{(2)}$	1.94 ± 0.09	1.82 ± 0.08	
$\tau_{oopl}^{(2)}$	1.50 ± 0.07	1.27 ± 0.05	~2[d]

[a] From ref 62. [b] The superscripts (1) and (2) refer to the decay times for the first- and second-order Legendre polynomials, respectively. The subscripts refer to the various unit vectors: μ for the permanent dipole vector, hh for the hydrogen–hydrogen vector, and oopl for the out-of-plane vector. [c] From ref 63. [d] From ref 64.

The same trend can be seen in the rotational dynamics of the water molecule. This can be examined by evaluating the reorientational correlation functions corresponding to the first and second Legendre polynomials

$$\langle P_1[\mathbf{e}_i(t)\cdot\mathbf{e}_i(0)]\rangle = \langle \mathbf{e}_i(t)\cdot\mathbf{e}_i(0)\rangle \qquad (14)$$

and

$$\langle P_2[\mathbf{e}_i(t)\cdot\mathbf{e}_i(0)]\rangle = {}^1/_2\langle 3[\mathbf{e}_i(t)\cdot\mathbf{e}_i(0)]^2 - 1\rangle \qquad (15)$$

where $\mathbf{e}_i$ is some unit vector. The correlation functions for the following vectors were examined: the permanent dipole vector, the H–H intramolecular vector, and the vector normal to the plane of the molecule. The functions for each of these vectors were assumed to undergo exponential decay, and the correlation decay times were determined via least-squares fitting. This fitting did not include results from the first 0.5 ps of the trajectory in order to omit the effects of hindered librations. The resulting correlation times are shown in Table 6. The values from simulations using the polarizable model are in good agreement with experimental results.

The all-atom polarizable potential describes the dynamics of bulk water more accurately than its nonpolarizable counterpart, the SPC model. Comparison of the computed correlation times indicates that the addition of polarizable sites slows the rotation of the molecule in solution. This is consistent with the slower rate of translational diffusion exhibited by the polarizable model—the addition of polarization retards both the rotational and translational motions. A similar effect was observed by Ahlström and co-workers[7] for their PSPC model, which places polarizable sites only on the oxygen atoms. The PSPC model was further studied by van Belle and co-workers,[65] who used a scaling function to decrease the electrostatic fields. This resulted in smaller induced dipoles and less retardation of the molecular motions in solution.

Why does the polarizable model predict more realistic dynamics (but similar structure) when compared to the nonpolarizable models? Sprik[11,12] has pointed out that unlike structural averages, which are dominated by fluctuations about configurations with the highest probability in the phase space, diffusion and molecular rotations are activated processes which depend on infrequent jumps over energy barriers. It is these barriers that influence the dynamics, and apparently the polarizable model provides a better description of these energy barriers. We can speculate as to the reason for this. The polarizable and nonpolarizable models are parametrized to give the same energy for the "ground" state. In

the transition state, the net polarization on the activated water molecule is likely to be smaller than in the ground state. If the dipole interaction energy of the activated water molecule is attractive, then allowing for the polarization to relax will reduce the electrostatic term and increase the barrier.

The retardation of rotational motions in simulations using our polarizable model and the PSPC model leads to another issue: Is there a difference between the predictions of a model which uses all-atom polarizabilities and a model which only has polarizable oxygen atoms? Both models predict similar induced and total dipole moments, yet ours gives shorter rotational correlation times which imply rotations which are faster than those of the PSPC model. One possible explanation for this difference is the following: The sole polarizable site in the PSPC model is on the oxygen, which is very close to the molecular center of mass. This means that the contribution of the induced dipole to the torque on the molecule is small. Our model, on the other hand, has polarizable sites on the hydrogen atoms as well. The induced dipoles on these atoms can make a contribution to the torque acting on the molecule, resulting in large average torques and rotational motions which are faster than those of the PSPC model.

The presence of polarizable sites on hydrogen atoms may also be important in describing specific hydrogen–heteroatom interactions such as hydrogen bonding. For example, in a study of proteins van Belle and co-workers[15] found that the largest electrostatic fields due to induced dipoles could be found on hydrogen and nitrogen atoms that formed hydrogen bonds with carboxylate groups. Hydrogen atoms not involved in hydrogen bonds had invariably lower induced fields.

One disadvantage of using an all-atom polarizable model is the increased computational effort required to compute the energies and forces due to the additional polarizable sites. The polarizable water simulations reported here were carried out on a Thinking Machines CM-5, which is a massively parallel computer. In the following section we discuss the implementation of the model on this machine.

4. Implementation on a Massively Parallel Computer. All the induced dipole moments in this study were calculated by matrix inversion of **A** (see eq 10). The 216-water system requires this inversion to be performed on a 1944 × 1944 matrix for every time step. These repeated operations are possible only on the most recent generation of massively parallel computers.[66] It is for this reason that earlier studies have obtained the induced dipole moments via an iterative procedure.[2,15] This procedure is faster than the matrix inversion approach but may introduce some error into the polarization energies and forces. Since no study of the two methods has been published, we have performed our own comparison. We repeated some of our calculations using the iterative approach as outlined by van Belle and co-workers.[15] The convergence criterion suggested by Kollman[2] was used: the iterations were continued until $\langle(\mu_m - \mu_{m-1})^2\rangle^{1/2} < 0.01$ D/atom was satisfied in the mth iteration.

Preliminary calculations on a 64-water system were done to assess the computational requirements of the two algorithms. On our Silicon Graphics 4D/340 (a SISD machine), the iterative approach was roughly 20 times faster than the matrix inversion method. However, a much smaller difference is 15–20% was observed when the calculations were done on a massively parallel CM-5 computer.

Matrix inversion appears to be a more efficient procedure on the CM-5 than it is on the SISD workstation. It is known[67] that the time required to invert an $N \times N$ matrix is proportional to N^3 when the inversion algorithm is performed sequentially (e.g., on a SISD machine). On the massively parallel computer, we have found that matrix inversion scales as $N^{1.5}$. This increased efficiency means that the matrix inversion approach becomes a practical alternative to the iterative approach when working with large matrices on a parallel computer. Since the differences in the computational requirements of the two methods are small, the choice of a particular algorithm can be based on scientific rather than computational grounds.

We have also found the matrix inversion approach to be more robust than the iterative procedure in calculating dipole moments for configurations where the distances between polarizable sites are small. While configurations such as these may be rarely encountered in simulations involving pure water, their occurrence in systems involving highly polar and/or ionic solutes will probably be more common. Furthermore, the use of an all-atom polarizable model such as ours increases the chances of having two polarizable sites close to each other. These configurations lead to relatively large induced dipoles, the values of which are not always accurately predicted by the simple iterative approach. We have found that matrix inversion always yields the correct values for the dipole moments in the above systems.

In order to examine differences in the physical predictions derived from the two algorithms, a 1-ps simulation was performed using the iterative approach. At each time step, U_{tot} and the atomic positions were compared to those of a reference system in which the induced dipole moments had been obtained by matrix inversion. Although there were differences in U_{tot} at each time step, the average values were statistically indistinguishable. As far as the prediction of potential energies and atomic positions are concerned, the results of the iterative approach are comparable to those of the matrix inversion approach.

In the interests of further reducing computational requirements, we examined the effects of using a cutoff distance in the evaluation of **A** and its derivatives. This would lead to changes in the forces. These changes were measured by evaluating $R_f = \langle|F_c - F_\infty|/|F_\infty|\rangle$, where the subscripts refer to cutoff values of c and ∞ (i.e., no cutoff). We found that $R_f = 2\%$ for $c = 6$ Å and $R_f = 5\%$ for $c = 4$ Å. It appears that cutoff distances of 4–6 Å for calculating the matrix elements of **A** can be used without a significant loss in accuracy.

IV. Conclusions

In this study we have developed an all-atom polarizable potential that is based on the combination of interacting point dipole polarizabilities on all atoms with the pairwise force field of the SPC model. No reparametrization of the pairwise functions other than the values of the partial atomic charges is necessary. In the resulting potential, both atomic polarizabilities and charges are damped at short interatomic distances. This attenuation corresponds to a more realistic treatment of the electronic charge spatial distribution; the assumption of point charges at these short distances leads to unreasonably large induced dipoles. The calculation of dipoles is free of singularities, which allows treatment of dipole–dipole interactions between bonded atoms and simplifies the incorporation of polarization treatments into existing molecular mechanics force fields.

Our potential correctly predicts the dipole moments of the water monomer and dimer. The potential also predicts the correct equilibrium geometry for the water trimer. Simulations on a 216-molecule system show that the polarizable potential yields bulk structure and energies that are in good agreement with experimental findings as well as predictions made with the widely used SPC model. This latter model is known to overestimate the translational and rotational velocities of molecules in the bulk. In comparison, the polarizable water model includes induced dipoles which retard the motion of the water molecules, leading to a diffusion constant and rotational lifetimes which are closer to the experimental values than those predicted by the SPC model.

The computational requirements associated with the calculation of induced dipole moments were also studied. It is known that the iterative solution to the calculation of induced dipoles is much faster than the matrix inversion approach when performed on a

single processor. However, it was found that run-time differences between the two became considerably smaller when calculations were done on a massively parallel CM-5 computer. Run times could be further shortened (with little loss of accuracy in the computed dipoles) by using cutoff distances of 4–6 Å in the construction of the dipole tensor matrix and its derivatives.

The polarizable potential that was developed in this study is well suited for all-atom molecular mechanics approaches to simulations of chemical systems. The extension of the all-atom polarizable water model to heterogeneous systems is the next logical step in our development of simulations with fully polarizable potentials. The attenuation of electric fields and damping of atomic polarizabilities at short ranges suggests that the polarizable potential will be singularity-free and stable even when used to study heterogeneous systems where polarization effects might be greater than those encountered in bulk water. This stability has been examined and verified in preliminary simulations on aqueous solutions of Cl^-, Na^+, NH_3, and *cis*- and *trans*-*N*-methylacetamide. More extensive studies are in progress. One kind of problem we are exploring involves conformational equilibria. An interesting example that has been discussed in the literature concerns the relative solvation free energies of *cis*- and *trans*-*N*-methylacetamide. In studies using nonpolarizable potentials, it has been shown that different sets of partial atomic charges for the *cis* and *trans* isomers are necessary in order to obtain the correct difference in the solvation free energies.[68,69] We have developed a consistent set of charges and polarizabilities for *N*-methylacetamide by simultaneously fitting these parameters to the quantum mechanical electrostatic potentials of the two isomers.[70] The resultant polarizabibilities are close to the atomic polarizabilities used by Thole. Simulations of *N*-methylacetamide in water using the polarizable potentials are underway. Since few simulations involving polarizable solutes in polarizable solvents have been carried out to date, the analysis of polarization effects on the solvation of organic and bioorganic systems will undoubtedly be the focus of many future studies as the available computational resources expand to allow the systematic study of this problem.

Acknowledgment. We thank Francisco Figueirido and John D. Westbrook for help with the calculations and for numerous lively discussions concerning this project. This work has been supported in part by grants from the National Science Foundation (DMB-9105208), the National Institutes of Health (GM30580), the Columbia University Center for Biomolecular Simulations (NIH P41 RR06892), and a grant of time at the National Center for Supercomputing Applications.

References and Notes

(1) Jorgensen, W. L.; Chandrasekhar, J.; Madura, J. D.; Impey, R. W.; Klein, M. L. *J. Chem. Phys.* **1983**, *79*, 926 and references therein.
(2) Caldwell, J.; Dang, L. X.; Kollman, P. A. *J. Am. Chem. Soc.* **1990**, *112*, 9144.
(3) Wallqvist, A.; Ahlström, P.; Karlström, G. *J. Phys. Chem.* **1990**, *94*, 1649.
(4) Stillinger, F. H.; David, C. W. *J. Chem. Phys.* **1978**, *69*, 1473.
(5) Halley, J. W.; Rustad, J. R.; Rahman, A. *J. Chem. Phys.* **1993**, *98*, 4110.
(6) Niesar, U.; Corongiu, G.; Clementi, E.; Kneller, G. R.; Bhattacharya, D. K. *J. Phys. Chem.* **1990**, *94*, 7949.
(7) Ahlström, P.; Wallqvist, A.; Engström, S.; Jönsson, B. *Mol. Phys.* **1989**, *68*, 563.
(8) Rullmann, J. A. C.; van Duijnen, P. Th. *Mol. Phys.* **1988**, *63*, 451.
(9) Straatsma, T. P.; McCammon, J. A. *Chem. Phys. Lett.* **1991**, *177*, 433.
(10) Sprik, M.; Klein, M. L. *J. Chem. Phys.* **1988**, *89*, 7556.
(11) Sprik, M. *J. Phys. Chem.* **1991**, *95*, 2283.
(12) Sprik, M. *J. Chem. Phys.* **1991**, *95*, 6762.
(13) Barnes, P.; Finney, J. L.; Nicholas, J. D.; Quinn, J. E. *Nature (London)* **1979**, *282*, 459.
(14) Levesque, D.; Weiss, J. J.; Patey, G. N. *Mol. Phys.* **1984**, *51*, 333.
(15) van Belle, D.; Couplet, I.; Prevost, M.; Wodak, S. J. *J. Mol. Biol.* **1987**, *198*, 721.
(16) (a) Rashin, A. A. *Int. J. Quantum Chem.: Quantum Biol. Symp.* **1988**, *15*, 103. (b) Rashin, A. A. *J. Phys. Chem.* **1990**, *94*, 1725.
(17) Sauniere, J. C.; Lybrand, T. P.; McCammon, J. A.; Pyle, L. D. *Comput. Chem.* **1989**, *13*, 313.
(18) Mertz, J. E.; Tobias, D. J.; Brooks III, C. L.; Singh, U. C. *J. Comput. Chem.* **1991**, *12*, 1270.
(19) Clark, T W.; McCammon, J. A.; Scott, L. R. In *Proceedings of the Fifth SIAM Conference on Parallel Computing*, in press.
(20) Wilson, M. A.; Pohorille, A.; Pratt, L. R. *J. Phys. Chem.* **1987**, *91*, 4873.
(21) Matsumoto, M.; Kataoka, Y. *J. Chem. Phys.* **1988**, *88*, 3233.
(22) Dang, L. X.; Rice, J. E.; Caldwell, J.; Kollman, P. A. *J. Am. Chem. Soc.* **1991**, *113*, 2481.
(23) Sprik, M.; Klein, M. L.; Watanabe, K. *J. Phys. Chem.* **1990**, *94*, 6483.
(24) Foresman, J. B.; Brooks III, C. L. *J. Chem. Phys.* **1987**, *87*, 5892.
(25) Luzhkov, V.; Warshel, A. *J. Comput. Chem.* **1992**, *13*, 199.
(26) Lee, F. S.; Chu, Z. T.; Warshel, A. *J. Comput. Chem.* **1993**, *14*, 161.
(27) Cramer, C. J.; Truhlar, D. G. *Science* **1992**, *256*, 213.
(28) van Belle, D.; Wodak, S. J. *J. Am. Chem. Soc.* **1993**, *115*, 647.
(29) Berne, B. J.; Wallqvist, A. *Chem. Scr.* **1989**, *29A*, 85.
(30) Wallqvist, A. *Chem. Phys. Lett.* **1990**, *165*, 437.
(31) Wallqvist, A. *J. Phys. Chem.* **1991**, *95*, 8921.
(32) Belford, D.; Campbell, E. S. *J. Chem. Phys.* **1987**, *86*, 7013.
(33) Dykstra, C. E. *J. Chem. Phys.* **1989**, *91*, 6472.
(34) (a) Perera, L.; Berkowitz, M. L. *J. Chem. Phys.* **1991**, *95*, 1954. (b) Jorgensen, W. L.; Severance, D. L. *J. Chem. Phys.* **1993**, *99*, 4233. (c) Perera, L.; Berkowitz, M. L. *J. Chem. Phys.* **1993**, *99*, 4236.
(35) Perera, L.; Berkowitz, M. L. *J. Chem. Phys.* **1992**, *96*, 8288.
(36) Thole, B. T. *Chem. Phys.* **1981**, *59*, 341.
(37) Applequist, J.; Carl, J. R.; Fung, K. K. *J. Am. Chem. Soc.* **1972**, *94*, 2952.
(38) Miller, K. J. *J. Am. Chem. Soc.* **1990**, *112*, 8543 and references therein.
(39) Berendsen, H. J. C.; Postma, J. P. M.; van Gunsteren, W. F.; Hermans, J. In *Intermolecular Forces*; Pullman, B., Ed.; Riedel: Dordrecht, Holland, 1981; p 331.
(40) Dyke, T. R.; Muenter, J. S. *J. Chem. Phys.* **1973**, *59*, 3125.
(41) Böttcher, C. J. F. *Theory of Electric Polarization*, 2nd ed.; Elsevier: Amsterdam, 1973.
(42) Berne, B. J.; Wallqvist, A. *J. Chem. Phys.* **1988**, *88*, 8016.
(43) Silberstein, L. *Philos. Mag.* **1917**, *33*, 92, 215.
(44) Miller, K. J. In *CRC Handbook of Chemistry and Physics*; Lide, D. R., Ed.; CRC Press: Boca Raton, 1993; p. 10–194.
(45) In contrast, use of an exponent such as $m = 8$ yields a 25% difference between w_{ij} and v_{ij} at $r_{ij}/s_{ij} = 0.5$.
(46) This is equivalent to the more obvious expression $\mathbf{F}_k = (1/2)\nabla_k[\sum_i \mu_i \mathbf{E}_i^0]$.
(47) Kuwajima, S.; Warshel, A. *J. Phys. Chem.* **1990**, *94*, 460.
(48) Kitchen, D. B.; Hirata, F.; Westbrook, J. D.; Levy, R. M.; Kofke, D.; Yarmush, M. *J. Comput. Chem.* **1990**, *11*, 1169.
(49) Odutola, J. A.; Dyke, T. R. *J. Chem. Phys.* **1980**, *72*, 5062.
(50) Curtiss, L. A.; Frurip, D. J.; Blander, M. *J. Chem. Phys.* **1979**, *71*, 2703.
(51) Pugliano, N.; Saykally, R. J. *Science* **1992**, *257*, 1937.
(52) Berendsen, H. J. C.; Postma, J. P. M.; van Gunsteren, W. F.; DiNola, A.; Haak, J. R. *J. Chem. Phys.* **1984**, *81*, 3684.
(53) Sopher, A. K.; Phillips, M. G. *Chem. Phys.* **1986**, *107*, 47.
(54) The magnitudes of the permanent and average induced dipole moments do not add up to 2.81 D. This is due to variations in the angle θ between the permanent and induced dipole vectors. We find that $\langle \cos \theta \rangle = 0.933$.
(55) Berendsen, H. J. C.; Grigera, J. R.; Straatsma, T. P. *J. Phys. Chem.* **1987**, *91*, 6269.
(56) Johari, G. P.; Whalley, E. *J. Chem. Phys.* **1976**, *64*, 4484. They obtain $\mu = 2.58$ D for ice IV but remark that μ^2 is probably underestimated by 10%, which implies a value of $\mu = 2.72$ D.
(57) Coulson, C. A.; Eisenberg, D. *Proc. R. Soc. London, Ser. A* **1966**, *291*, 445.
(58) Whalley, E. *Chem. Phys. Lett.* **1978**, *53*, 449.
(59) Onsager, L.; Dupuis, M. In *Electrolytes*; Pesce, B., Ed.; Pergamon: London, 1962.
(60) Alper, H. E.; Levy, R. M. *J. Chem. Phys.* **1989**, *91*, 1242.
(61) Alper, H. E.; Levy, R. M. *J. Chem. Phys.* **1993**, *99*, 9847.
(62) Krynicki, K.; Green, C. D.; Sawyer, D. W. *Discuss. Faraday Soc.* **1978**, *66*, 199.
(63) Eisenberg, D.; Kauzman, W. *The Structure and Properties of Water*; Oxford University Press: Oxford, 1969; p 207.
(64) Halle, B.; Wennerström, H. *J. Chem. Phys.* **1972**, *75*, 1928.
(65) van Belle, D.; Froeyen, M.; Lippens, G.; Wodak, S. J. *Mol. Phys.* **1992**, *77*, 239.
(66) Cao, J.; Berne, B. J. *Theory of Polar Polarizable Fluids*, preprint.
(67) Press, W. H.; Flannery, B. P.; Teukolsky, S. A.; Vetterling, W. T. *Numerical Recipes: The Art of Scientific Computing*; Cambridge University Press: New York, 1986; pp 37–38, 74–76.
(68) Jorgensen, W. L.; Gao, J. *J. Am. Chem. Soc.* **1988**, *110*, 4212.
(69) Cieplak, P.; Kollman, P. *J. Comput. Chem.* **1991**, *12*, 1232.
(70) Westbrook, J. D.; Ding, Y.; Figueirido, F., private communication.